

Article

Injection Harmonic Current Differential Protection Based on Control-Protection Synergy for Distribution Networks with IBDGs

Chengao Yu, Zhanjun Gao *, Zhao Liu and Zhengchen Tao

Key Laboratory of Power System Intelligent Dispatch and Control of Ministry of Education, Shandong University, Jinan 250061, China; 202134719@mail.sdu.edu.cn (C.Y.); 202134661@mail.sdu.edu.cn (Z.L.); 202234733@mail.sdu.edu.cn (Z.T.)

* Correspondence: jacob-gao@sdu.edu.cn; Tel.: +86-131-8889-0434

Abstract: The high penetration of inverter-based distributed generations (IBDGs) leads to traditional distribution networks' complex and variable fault characteristics. Traditional passive detection protection methods can hardly meet the stability and reliability requirements. To solve this problem, an injection harmonic current differential protection (IHCDP) scheme based on the idea of control-protection synergy is proposed in this paper. By analyzing the circuit structure, control strategy, low-voltage-ride-through characteristics of IBDGs, and short-circuit currents provided by IBDGs, an injection-control strategy of characteristic harmonic currents (CHCs) based on the d-axis and q-axis is proposed. According to the change of short-circuit currents provided by the IBDG, the amplitude of CHCs is adaptively corrected to strengthen the fault characteristics and ensure that the distribution network harmonic injection protocols are always satisfied. An IHCDP criterion based on the distortion rate of the negative-sequence component of CHCs is proposed by analyzing the fault characteristics of the CHCs after injection. To effectively eliminate the dead-zone problem during symmetrical short-circuit faults, the proposed IHCDP utilizes the distortion rate of A-phase CHCs. The feasibility of the proposed protection scheme is demonstrated by the theoretical analysis and simulation results in this paper.

Keywords: distribution networks with IBDGs; control-protection synergy; characteristic harmonic currents; injection current differential protection



Citation: Yu, C.; Gao, Z.; Liu, Z.; Tao, Z. Injection Harmonic Current Differential Protection Based on Control-Protection Synergy for Distribution Networks with IBDGs. *Appl. Sci.* **2023**, *13*, 6725. <https://doi.org/10.3390/app13116725>

Received: 11 May 2023
Revised: 28 May 2023
Accepted: 30 May 2023
Published: 31 May 2023



Copyright: © 2023 by the authors. Licensee MDPI, Basel, Switzerland. This article is an open access article distributed under the terms and conditions of the Creative Commons Attribution (CC BY) license (<https://creativecommons.org/licenses/by/4.0/>).

1. Introduction

After a large number of distributed generations (DGs) are connected to the distribution network, the topology of the traditional distribution network has been dramatically transformed from the original single-power supply radial network structure to a complex network structure with multiple-power supplies. The operation mode, power flow, and short-circuit current fault characteristics of the distribution network are complex and variable [1], making its protection face significant challenges [2].

Depending on the grid-connected interface, DGs can be divided into synchronous-based DGs (SBDGs) directly connected to the grid and IBDGs connected to the grid by inverters [3]. Among them, the fault characteristics of IBDGs differ from traditional synchronous generators due to the low inertia, high controllability, and poor overcurrent capability of inverters [4]. The output currents of IBDGs are affected by their inverter control strategy, low voltage ride-through (LVRT), and fault conditions. The uncertainty of IBDGs' output currents makes the setting and delay coordination of traditional passive-detection-type protection face significant challenges in the distribution network with IBDGs [5], especially in the case of high penetration of IBDGs.

Most available studies have improved traditional passive-detection protection methods to make them applicable to distribution networks with DGs. Traditional overcurrent

protection is improved in [6–8], modifying the protection setting values according to the DG output's fault characteristics. This method is simple to implement and has high sensitivity. However, it is difficult to set and coordinate the protection in the active distribution network due to its variable operation modes, complex branches, and numerous DG access points. To solve the above problems, an overcurrent protection scheme based on wide-area communication is proposed in [9–12]. After receiving current information, the centralized controller adaptively calculates the set value of each protection, which requires high communication requirements. In [13], an efficient protection method is proposed by comprehensively using the local fault voltage and current information without communication, but is only applicable to the distribution network with SBDGs.

Compared with single-end protection based on local information, pilot protection using electrical information at both ends of the feeder has superior operational performance in multi-power networks. Adjacent impedance information is used to construct protection criteria in [14–16] for fault identification and isolation with high protection reliability. All of the above methods use voltage information. However, the practical medium/low voltage distribution network feeders are generally not equipped with voltage transformers, which limits the application of these schemes. In [17,18], current differential protection applied in transmission lines is improved and introduced into the distribution network, which has good selectivity, but high requirements for data time synchronization.

Traditional passive protection methods seldom consider the influence of the control strategy of IBDG. However, the control strategy of IBDG directly determines its fault characteristics, which is critical for protection. In [19], the idea of control-protection synergy is first proposed: fault detection is achieved using the control strategy of the IBDG. In [20], a protection scheme based on controlling the negative-sequence current of the IBDG output is proposed, but fault types must be judged first to determine the given value of the negative-sequence current. Reference [21] reviews active detection-based fault identification methods, and the feasibility and physical limitations of the injection detection signal operation are described. In [22], a differential protection scheme based on non-rated frequency injection is proposed to detect and isolate faults. In [23], an overcurrent protection scheme based on harmonic voltage injection is proposed, and fault detection and isolation are achieved by integrating the amplitude and phase of harmonic currents. The methods proposed in [22,23] mainly apply to microgrids under islanding operation mode. However, they provide a new idea for studying control-protection synergy in active distribution networks: active injection detection type protection.

Considering that the system power supply will generate harmonics during faults in the distribution network and the distribution network has strict requirements for harmonic injection, whether the injection protection method can be applied to the distribution network needs further study. This paper revisits the feasibility of active injection detection protection in distribution networks with IBDGs and proposes an injection harmonic current differential protection (IHCDP) scheme based on control-protection synergy. The remainder of this paper is organized as follows. Section 2 deeply studies the equivalent model of IBDG, including its circuit structure, control strategy, and LVRT characteristics. Section 3 analyzes the change of short-circuit currents provided by IBDG before and after injecting characteristic harmonic signals. Section 4 describes the principle of IHCDP. On this basis, the implementation scheme of IHCDP is presented in Section 5. The feasibility of the proposed protection scheme is verified by PSCAD/EMTDC in Section 6. Section 7 summarizes the results and the contributions of this paper.

2. Equivalence Model of IBDG

2.1. Typical Structure of IBDG

The fault characteristics of the distribution network with IBDGs are closely related to the fault response of IBDGs, so it is necessary to study the typical structure and control strategy of IBDGs in depth before designing an injection protection scheme.

The typical structure of IBDG operating at the fundamental frequency signal consists of three parts [24]: the DC source, power electronic inverter, and filter circuit, as shown in Figure 1a. C_{dc} is the DC voltage regulator capacitor, R_f is the filter resistor, L_f is the filter inductor, and C_f is the filter capacitor.

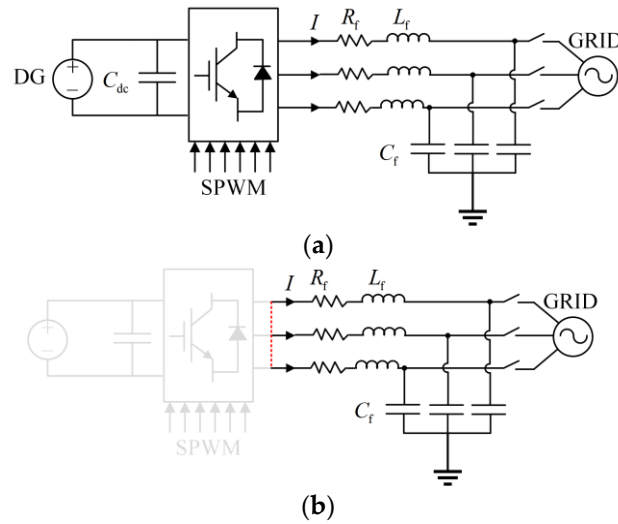


Figure 1. Typical structure of IBDG (a) under fundamental frequency signals, and (b) under characteristic frequency signals.

The frequency of characteristic signals selected by existing injection protection schemes is generally far from the fundamental frequency (50 Hz). For the IBDG operating at the fundamental frequency signal, the gain of its controller on the characteristic signal is meager. It can be assumed that the outlet voltage of the IBDG inverter does not contain the characteristic frequency signal. Therefore, regardless of the control strategy of the IBDG, for the characteristic frequency signal, the IBDG can be equated to an RLC parallel circuit, as shown in Figure 1b.

The resonant frequency of the RLC parallel circuit shown in Figure 1b can be derived as

$$f_c = \frac{1}{2\pi\sqrt{L_f C_f}} \sqrt{1 - \frac{C_f R_f^2}{L_f}} \quad (1)$$

where f_c is the resonant frequency, whose value is determined by the filter parameters R_f , L_f , and C_f .

2.2. PQ Control Strategy of IBDGs

Most IBDGs in the existing distribution network are controlled by a constant power (PQ) control strategy [25]. Under normal operation, the control system directs the universal voltage phasor of the grid connection point to the d-axis (assuming that the d-axis phase is ahead of the q-axis phase). The power outer loop control link of the PQ control strategy can be expressed as [26,27].

$$\begin{cases} P_{out} = P_{ref} = \frac{3}{2} U_{pcc_d} I_{d_ref} \\ Q_{out} = Q_{ref} = \frac{3}{2} U_{pcc_d} I_{q_ref} \end{cases} \quad (2)$$

where, P_{out} and Q_{out} are the active and reactive power provided by the IBDG and P_{ref} and Q_{ref} are the given active and reactive reference power. To maximize the use of clean energy, the IBDG is usually constrained to output only active power, i.e., such that $Q_{out} = Q_{ref} = 0$; U_{pcc_d} is the d-axis component of the universal voltage phasor of the grid connection point; and I_{d_ref} and I_{q_ref} are the current reference values of the d-axis and q-axis in the current inner loop control link, representing the active and reactive currents, respectively.

2.3. Control Characteristics of Low Voltage Ride-Through

According to the new international and Chinese standards for grid connection [28,29], medium and large IBDGs must have LVRT capability. When the grid is disturbed, or a fault occurs, IBDGs need to inject reactive current as a priority to support the grid voltage during LVRT. Taking the standard of the latest Chinese grid connection as an example, the dynamic reactive current injected during LVRT operation can be expressed as [29,30]

$$I_{q_ref} = \begin{cases} 0 & , 0.9 < U_{pcc}^* \\ \min \left\{ K_1 (0.9 - U_{pcc}^*) I_N, I_{max} \right\} & , 0.2 \leq U_{pcc}^* \leq 0.9 \\ K_2 I_N & , U_{pcc}^* < 0.2 \end{cases} \quad (3)$$

where I_{q_ref} is the reference value of the injected reactive current during LVRT; U_{pcc}^* is the per-unit value of grid connection point voltage; K_1 is the reactive support factor, $K_1 \geq 1.5$; K_2 determines the maximum value of reactive current injection at low voltage, $K_2 \geq 1.05$; and I_N is the output rated current of IBDG; I_{max} is the maximum fault current allowed to be output by the IBDG, generally limited to two times the rated current. From Equation (3), when U_{pcc}^* is greater than 0.9, $I_{q_ref} = 0$, the IBDG outputs only active current; when U_{pcc}^* drops to the range of 0.2–0.9, in order to support the system voltage, the IBDG should output as much reactive current as possible, providing at least 1.5% reactive current for every 1% voltage drop while not exceeding the maximum allowable current output by the IBDG; when U_{pcc}^* is less than 0.2, the maximum reactive current value allowed to be output by the IBDG is $K_2 I_N$, whose value is equal to the value of reactive current output when $U_{pcc}^* = 0.2$.

In addition, as much active power should be output during the LVRT as possible while satisfying the reactive power output. In summary, the output current of IBDG can be expressed as [31]

$$\begin{cases} I_{IBDG_q} = I_{q_ref} \\ I_{IBDG_d} = \min \left\{ \frac{2P_{ref}}{3U_{pcc_d}}, \sqrt{(I_{max})^2 - (I_{q_ref})^2} \right\} \\ I_{IBDG} = \sqrt{(I_{IBDG_q})^2 + (I_{IBDG_d})^2} \end{cases} \quad (4)$$

where, I_{IBDG_d} and I_{IBDG_q} are the active and reactive currents provided by IBDG, respectively, and I_{IBDG} is the amplitude of the output current of IBDG. From Equation (4), the LVRT control strategy of IBDG gives priority to reactive power output, and the output of the reactive current tracking reference value should be ensured first. In order for the inverter to emit the maximum active power without exceeding the maximum allowed current, the active current reference is taken as the smaller value between $\frac{2P_{ref}}{3U_{pcc_d}}$ and $\sqrt{(I_{max})^2 - (I_{q_ref})^2}$ [26].

When the grid operates asymmetrically, the IBDG generates negative-sequence currents. Negative-sequence currents for control systems of IBDGs based on the synchronous rotating frame can deteriorate the control system performance, increase inverter losses, and exacerbate the degree of grid asymmetry. Therefore, most IBDGs adopt the PQ control strategy while suppressing the negative-sequence components. The electrical quantities in Equations (2)–(4) refer to the positive-sequence components.

3. Analysis of Output Short-Circuit Currents of IBDG

3.1. Analysis of Output Fundamental Frequency Short-Circuit Currents

According to the analysis in Section 2, the phase relationship between the universal phasor I_{IBDG} of the IBDG output current and the universal phasor U_{pcc_d} of positive-sequence voltage at the grid connection point can be obtained, as shown in Figure 2.

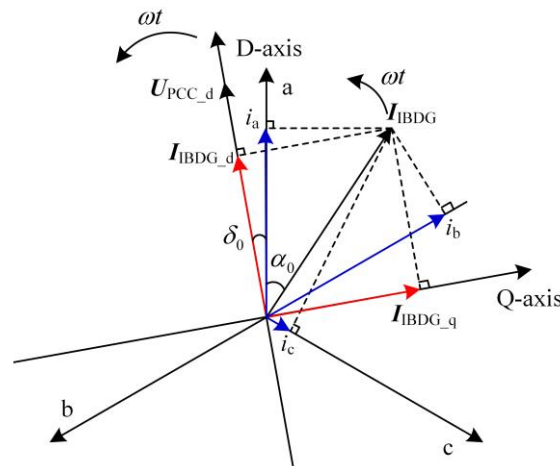


Figure 2. The phase relationship between I_{IBDG} and $U_{pcc,d}$.

After faults occur, the IBDG mainly outputs inductive reactive power [32], i.e., the $U_{pcc,d}$ phase is ahead of the I_{IBDG} phase. According to the phase relationship in Figure 2, the instantaneous values of the three-phase current provided by the IBDG can be found as

$$\begin{cases} i_a = I_{IBDG} \cos(\omega t + \alpha_0) \\ i_b = I_{IBDG} \cos(\omega t + \alpha_0 + 120^\circ) \\ i_c = I_{IBDG} \cos(\omega t + \alpha_0 - 120^\circ) \end{cases} \quad (5)$$

where, I_{IBDG} and α_0 are the amplitude and initial phase of the IBDG output current universal phasor I_{IBDG} , respectively, and ω is the grid angular frequency.

By triangulating the A-phase instantaneous current in Equation (5), it can be expressed as

$$\begin{aligned} i_a &= I_{IBDG} \cos((\delta_0 - \alpha_0) - (\omega t + \delta_0)) \\ &= I_{IBDG,d} \cos(\omega t + \delta_0) + I_{IBDG,q} \sin(\omega t + \delta_0) \end{aligned} \quad (6)$$

where δ_0 is the initial phase of $U_{pcc,d}$, due to suppressing negative-sequence currents, the three-phase current provided by the IBDG is symmetrical.

According to Equation (6), the instantaneous values of B-phase and C-phase currents expressed in terms of d-axis and q-axis components can be introduced as

$$\begin{cases} i_b = I_{IBDG,d} \cos(\omega t + \delta_0 - 120^\circ) + I_{IBDG,q} \sin(\omega t + \delta_0 - 120^\circ) \\ i_c = I_{IBDG,d} \cos(\omega t + \delta_0 + 120^\circ) + I_{IBDG,q} \sin(\omega t + \delta_0 + 120^\circ) \end{cases} \quad (7)$$

From Equations (5)–(7), I_{IBDG} can be derived as

$$I_{IBDG} = \sqrt{(I_{IBDG,q})^2 + (I_{IBDG,d})^2} \angle \alpha_0 \quad (8)$$

According to the phasor relation in Figure 2, it can be seen that

$$\alpha_0 = \arg(I_{IBDG,d} - jI_{IBDG,q}) + \delta_0 \quad (9)$$

3.2. Analysis of Output Short-Circuit Currents after Injection

At the instant after faults, it is assumed that the characteristic frequency signals $a \cos \theta_1$ and $a \sin \theta_1$ are injected into the d-axis and q-axis reference currents of the current internal loop control link in the IBDG control system, respectively. The instantaneous values

of the three-phase current provided by IBDG after injection are obtained according to Equations (5) and (6), and Park transformation, as shown in Equation (10).

$$\begin{aligned} \begin{bmatrix} i'_a \\ i'_b \\ i'_c \end{bmatrix} &= \begin{bmatrix} \cos \theta & \sin \theta \\ \cos(\theta - 120^\circ) & \sin(\theta - 120^\circ) \\ \cos(\theta + 120^\circ) & \sin(\theta + 120^\circ) \end{bmatrix} \begin{bmatrix} I_{IBDG_d} + a \cos \theta_1 \\ I_{IBDG_q} + a \sin \theta_1 \end{bmatrix} \\ &= \begin{bmatrix} I_{IBDG_d} \cos \theta + I_{IBDG_q} \sin \theta + a \cos(\theta_1 - \theta) \\ I_{IBDG_d} \cos(\theta - 120^\circ) + I_{IBDG_q} \sin(\theta - 120^\circ) + a \cos(\theta_1 - \theta + 120^\circ) \\ I_{IBDG_d} \cos(\theta + 120^\circ) + I_{IBDG_q} \sin(\theta + 120^\circ) + a \cos(\theta_1 - \theta - 120^\circ) \end{bmatrix} \end{aligned} \quad (10)$$

where, $\theta = \omega t + \delta_0$, $\theta_1 = \omega_1 t$, ω_1 is the characteristic angular frequency and a is the amplitude of the injected characteristic frequency signal.

Comparing Equations (5), (6) and (9), after injection, there will be new characteristic frequency signals in the output currents of IBDG. The new characteristic frequency signals are also called characteristic harmonic currents (CHCs). They are three-phase symmetrical. Taking the output current of the A-phase as an example analysis, the CHC is

$$a \cos(\theta_1 - \theta) = a \cos((\omega_1 - \omega)t - \delta_0) = a \cos(2\pi(f_1 - f)t - \delta_0) \quad (11)$$

where f_1 is the frequency of the characteristic signals injected into the d-axis and q-axis reference currents; f is the fundamental frequency. From Equation (11), the amplitude of the CHC is a , and the frequency of CHC is $(f_1 - f)$ Hz.

4. Principle of Characteristic Harmonic Current Differential Protection

Protection adopts three-phase reclosing in distribution networks, which does not need to determine the fault type. To reduce the amount of data transmitted by communication, this paper prioritizes the sequence component to construct the protection criterion. The CHCs in the short-circuit currents on the IBDG side are decomposed to obtain the positive, negative, and zero sequence components, as shown in Equation (12).

$$\begin{aligned} \begin{bmatrix} i^0 \\ i^+ \\ i^- \end{bmatrix} &= \frac{1}{3} \begin{bmatrix} 1 & 1 & 1 \\ 1 & 1\angle 120^\circ & 1\angle -120^\circ \\ 1 & 1\angle -120^\circ & 1\angle 120^\circ \end{bmatrix} \begin{bmatrix} a\angle -\delta_0 \\ a\angle(-\delta_0 + 120^\circ) \\ a\angle(-\delta_0 - 120^\circ) \end{bmatrix} \\ &= \begin{bmatrix} 0 \\ 0 \\ a\angle -\delta_0 \end{bmatrix} \rightarrow \begin{bmatrix} i^0 \\ i^+ \\ i^- \end{bmatrix} = \begin{bmatrix} 0 \\ 0 \\ a \cos((\omega_1 - \omega)t - \delta_0) \end{bmatrix} \end{aligned} \quad (12)$$

As seen from Equation (12), the decomposed CHCs contain only the negative-sequence component. The following is an analysis of the negative-sequence component of the characteristic harmonic currents (NSCCHCs) in the short-circuit currents.

In Figure 3, R_1 and R_2 are protective relays. After a fault occurs at point f , both the short-circuit currents provided by the GRID and the short-circuit currents provided by the IBDG flow to point f . The short-circuit currents at R_2 contain the injected CHCs, while the short-circuit currents at R_1 do not contain or contain fewer CHCs. In order to reduce the interference caused by the harmonics generated at the moment of fault, this paper constructs the differential protection criterion based on the distortion rate of NSCCHCs. The distortion rate of the NSCCHC is defined as

$$DR_f(h) = \frac{I_f(h)}{I_f(1)} \quad (13)$$

where $I_f(h)$ is the amplitude of the NSCCHC; $I_f(1)$ is the amplitude of the negative-sequence component of the fundamental frequency current (NSCFFC). The calculation of the distortion rate of the A-phase CHC is similar to this and will not be repeated here.

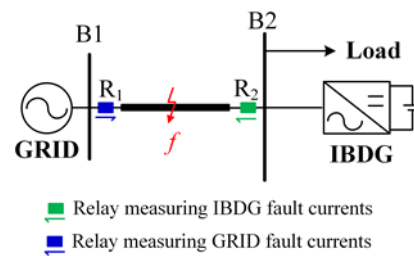


Figure 3. Schematic diagram of the distribution network with IBDG.

It should be noted that when symmetrical faults occur, NSCFCCs are about 0 within a short time after faults, and the differential protection criterion based on the distortion rate of NSCCHC is no longer applicable. In order to effectively eliminate the dead-zone problem of this criterion in symmetrical faults, the difference in the distortion rate of the A-phase CHCs on both sides of the protected feeder is used as an additional criterion. In summary, the injection CHC differential protection criteria are as follows.

- In the case of asymmetrical faults:

$$\Delta DR_f = \left| DR_{fGRID}(h) - DR_{fIBDG}(h) \right| > \Delta DR_{fset} \quad (14)$$

where, $DR_{fGRID}(h)$ and $DR_{fIBDG}(h)$ are the distortion rates of NSCCHCs on the GRID and IBDG sides of the protected feeder, respectively.

- In the case of symmetrical faults:

$$\Delta DR_A = \left| DR_{AGRID}(h) - DR_{AIBDG}(h) \right| > \Delta DR_{Aset} \quad (15)$$

where, $DR_{AGRID}(h)$ and $DR_{AIBDG}(h)$ are the distortion rates of A-phase CHCs on the GRID and IBDG sides of the protected feeder, respectively.

In Equations (14) and (15), ΔDR_{fset} and ΔDR_{Aset} are the action thresholds of the CHC differential protection criteria, generally taken as 0.3–0.5 times the total harmonic current distortion rate at the IBDG outlet.

5. Implementation Scheme of Injection Harmonic Current Differential Protection

5.1. Selection of the Frequency and Amplitude of the Characteristic Harmonic Current

For the injection protection scheme, the selection of the frequency of the CHC is crucial, and the following constraints need to be considered.

1. The characteristic frequency should not exceed ten times the fundamental frequency. The resonant frequencies of IBDG filters are generally widely distributed from 10 times the fundamental frequency to 0.5 times the carrier frequency. The characteristic frequency is less than ten times the fundamental frequency, which can avoid the resonance of CHCs with IBDG filters and thus ensure the safe and stable operation of IBDG. In order to suppress the shunting effect of the non-injected source IBDG on CHCs, the characteristic frequency cannot be much smaller than the resonant frequency.
2. The characteristic frequency should be as far from the fundamental frequency as possible. When the distribution network is disturbed, or after a fault occurs, the harmonics will inevitably be generated, mainly low-order harmonics. If the characteristic frequency is far from the fundamental frequency, it can minimize the interference of the generated harmonics to the injection protection.
3. The characteristic frequency should be taken as an integer multiple of the fundamental frequency. The selection of integer multiples of the fundamental frequency facilitates the extraction, analysis, and processing of the Fast Fourier Transform (FFT), wavelet transform, and other standard time-frequency analysis methods, shortens the signal

processing delay, and improves the engineering practicality of the injection protection method.

For the selection of the amplitude of the CHC, according to the latest Chinese regulations [33], the total harmonic distortion rates of the current injected into the grid are limited to 5% when the grid-connected inverter is operating at rated power. Therefore, the amplitude of the injected CHC needs to be less than 5% of the output current of IBDG.

In this paper, the eighth harmonic (with a frequency of 400 Hz) currents are injected into the d-axis and q-axis reference currents of the IBDG current inner loop control link. There will be seventh harmonic (with a frequency of 350 Hz) currents in the output currents of IBDG. The CHC injected into the grid remains at 4% of the IBDG output current amplitude in normal operation and under various fault scenarios. The amplitude a of the characteristic harmonic current should satisfy the following relation.

$$a = 4\% \times \sqrt{(I_{d_ref})^2 + (I_{q_ref})^2} \tag{16}$$

5.2. Principle of Injection Starting of Characteristic Harmonic Currents

In order to avoid harm to users from the CHCs injected under normal operation of the distribution network, this paper designs a corresponding starting module to initiate the injection of CHCs only after a fault. From Figure 4, the fault is detected by collecting the phase voltage and current at the IBDG outlet. When the starting criterion is satisfied, an enable signal is injected into the internal harmonic injection unit of the IBDG controller.

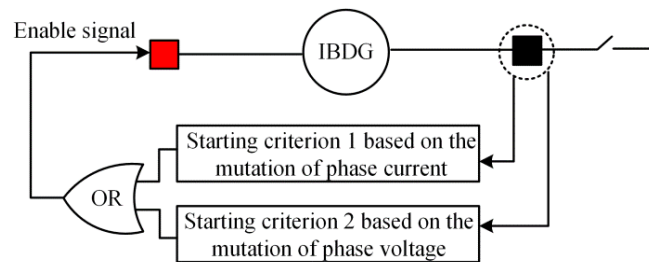


Figure 4. Starting schematic of the IBDG injection unit.

In Figure 4, the starting criterion 1 based on the mutation of phase current is as follows:

$$||i(k) - i(k - N)| - |i(k - N) - i(k - 2N)|| \geq K_S I_N \tag{17}$$

where $i(k)$ is the sampling value of phase current at time k ; N is the total number of sampling points per cycle; K_S is the starting coefficient and takes the value of 0.1–0.3; I_N is the rated current of the protected feeder; and “| |” are the signs for absolute value. The starting criterion 2 based on the mutation of phase voltage is similar to the starting criterion 1 and will not be repeated here.

5.3. Total Control System of IBDG with the CHC Injection

In Figure 5, the letters in the upper right corner of each module represent:

(a) the positive and negative-sequence separation link, which uses the delayed signal cancellation method [34] to realize the positive- and negative-sequence separation of electrical quantities;

(b) the PQ control link based on positive-sequence components, with power control in the outer loop and current control in the inner loop;

(c) the control link for suppressing negative-sequence currents;

(d) the LVRT link; and

(e) the fault detection and harmonic injection control link.

From Figure 5, when a fault occurs in the distribution network, module (e) of the IBDG control system detects the fault and injects an enable signal to module (b); after receiving

the enable signal, module (b) injects characteristic harmonic signals into the d-axis and q-axis reference currents of the current inner loop control link, respectively. The amplitude of characteristic harmonic signals adaptively changes with the output currents of IBDG, always keeping it at 4% of the amplitude of output currents, so that it can strengthen the fault characteristics and still meet the grid connection regulations under fault conditions, and finally completes the CHCs injection. The implementation process of the injection harmonic current differential protection scheme is shown in Figure 6.

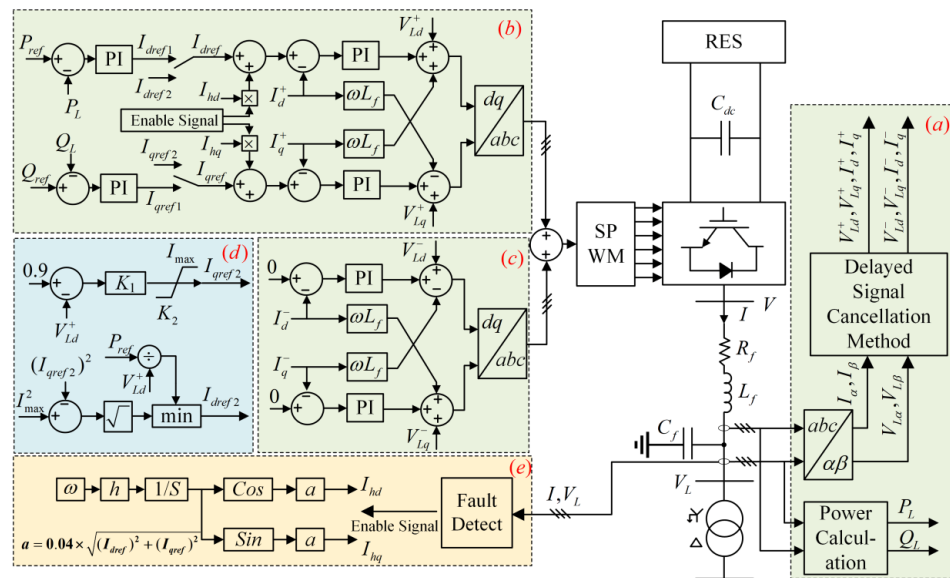


Figure 5. Overall control system structure of IBDG.

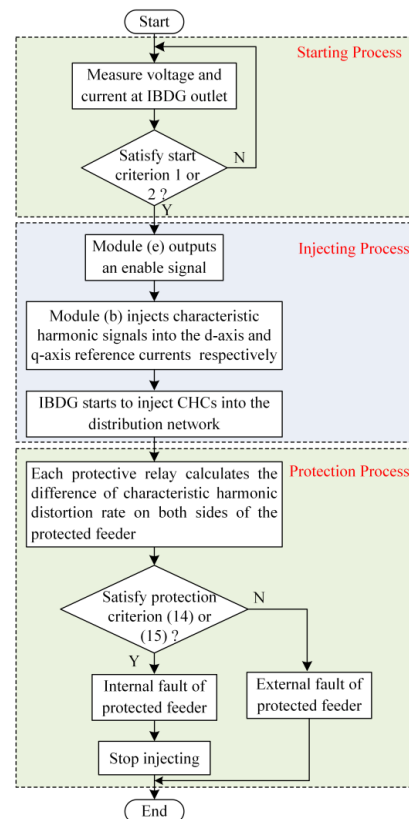


Figure 6. Implementation flowchart of the injection harmonic current differential protection scheme.

6. Simulation and Analysis

6.1. Test System under Study

To test the performance of the proposed protection scheme, a 10 kV distribution network with IBDGs simulation model was built using PSCAD/EMTDC, as shown in Figure 7. According to the China National Standard [35], the test system has three voltage levels: 35 kV (GRID), 10 kV (medium-voltage distribution network) and 0.38 kV (IBDGs). In Figure 7, GRID is the grid source; B1, B2, and B3 represent system buses; L1, L2, and L3 represent loads; R1, R2, R3, and R4 represent protective relays; and points f_1 and f_2 are located at the midpoints of feeder sections B1B2 and B2B3. The IBDGs in the test system adopt the PQ control strategy in Section 2 and have a low-voltage ride-through function. When asymmetric faults occur, the IBDGs can suppress the output of negative-sequence currents. In addition, the maximum output currents of IBDGs are 1.5 times the rated currents. The parameters of this simulation model are given in Table 1.

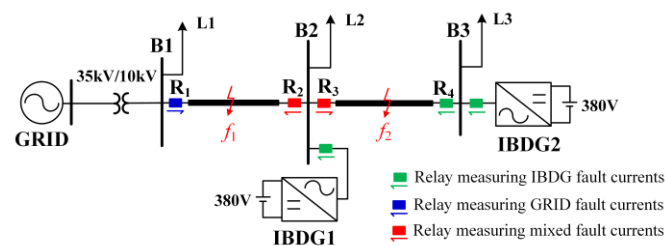


Figure 7. Simulation model of 10 kV distribution network with IBDGs.

Table 1. Parameters of the simulation model.

Parameters	Values
Capacity of IBDG1 and IBDG2	1 MW
Capacity of L1, L2 and L3	2 MVA
Length of feeder sections B1B2 and B2B3	4 km
Positive-sequence impedance of feeder sections B1B2 and B2B3	$(0.13 + j0.402) \Omega/\text{km}$
Negative-sequence impedance of feeder sections B1B2 and B2B3	$(2.00 + j0.400) \Omega/\text{km}$

6.2. Verifying the Correctness of CHCs Injection

6.2.1. During Normal Operation, CHCs Are Artificially Injected at 0.3 s

Under the normal operation of the distribution network with IBDGs, IBDG1 and IBDG2 artificially start injecting CHCs at 0.3 s according to the injection strategy in Section 5. The currents at the outlet of IBDG1 before and after injection are shown in Figure 8. The amplitude of the A-phase fundamental frequency current and CHC (350 Hz) are extracted using the FFT, and the distortion rate of A-phase CHC is calculated. The distortion rate of A-phase CHC at the IBDG1 outlet is shown in Figure 9. Figure 10 shows the amplitude Mag_{17} of A-phase CHC and the waveforms of characteristic harmonic (400 Hz) signals I_{hd} and I_{hq} injected d-axis and q-axis reference currents.

From Figure 8, it can be seen that there is a harmonic component in the current at the outlet of IBDG1 after 0.3 s, and this harmonic component is analyzed by using FFT. Due to the inherent delay of the FFT operation, the amplitude of the detected characteristic harmonic current reaches stability after one cycle (0.02 s), and its stable value is approximately equal to the amplitude of characteristic harmonic signals, as shown in Figure 10. As shown in Figure 9, the distortion rate of CHC at the outlet of IBDG1 is stabilized at 4% after one cycle, which meets the harmonic injection regulation of the distribution network. The above simulation results are consistent with the theoretical analysis in Section 3 and can verify the correctness of the CHCs injection system under normal operation.

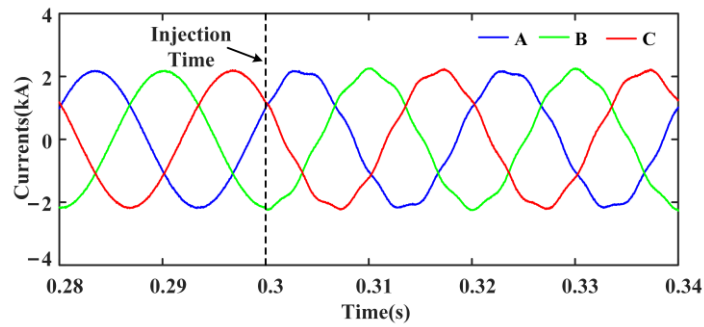


Figure 8. Currents at the outlet of IBDG1 before and after injection.

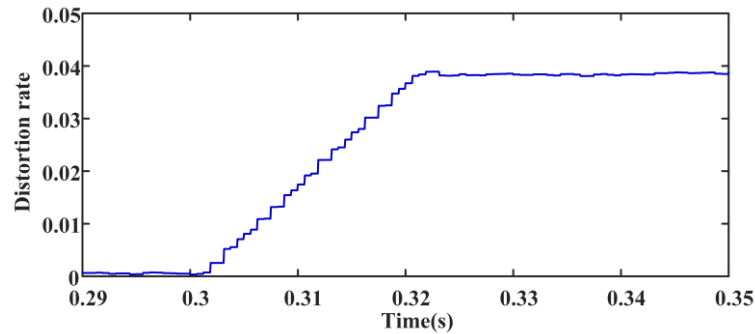


Figure 9. Distortion rate of A-phase CHC at the outlet of IBDG1.

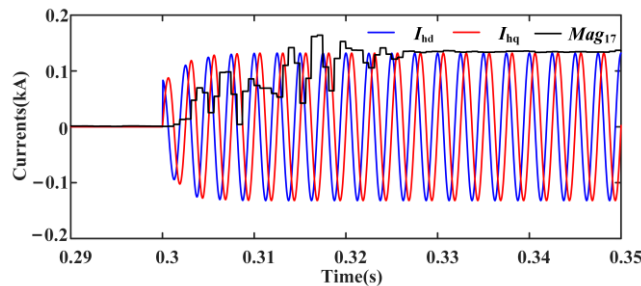


Figure 10. The amplitude of A-phase CHC and the waveforms of characteristic harmonic signals.

6.2.2. Phase-to-Phase (A–B) Faults with 0.1Ω Fault Resistance Occur at f_2

When a phase-to-phase (A–B) fault with 0.1Ω fault resistance occurs at f_2 , IBDG1 and IBDG2 detect the fault and initiate the injection of CHCs according to the injection strategy. The currents at the outlet of IBDG1 before and after the fault are shown in Figure 11. The distortion rate of A-phase CHC at the IBDG1 outlet is shown in Figure 12. The amplitude Mag_{17} of A-phase CHC and the characteristic harmonic signals I_{hd} and I_{hq} are shown in Figure 13.

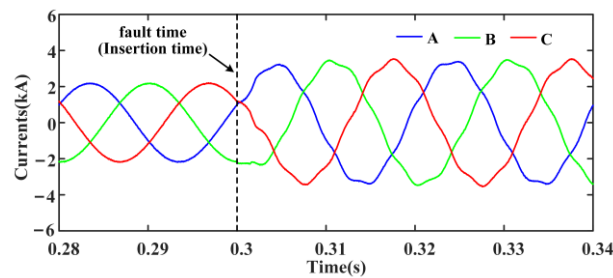


Figure 11. Currents at the outlet of IBDG1 before and after the fault.

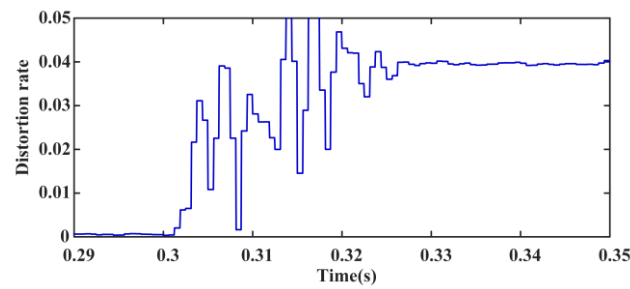


Figure 12. Distortion rate of A-phase CHC at the outlet of IBDG1 before and after the fault.

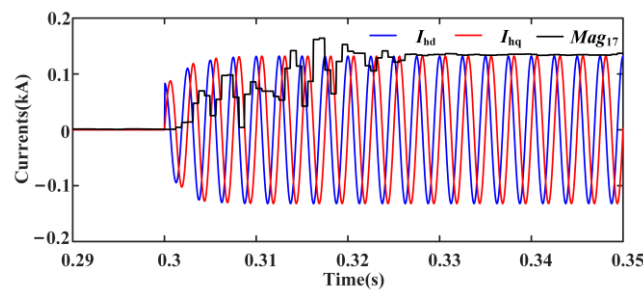


Figure 13. The amplitude of A-phase CHC and the waveforms of characteristic harmonic signals under the fault.

From Figure 11, IBDG1 performs LVRT at 0.3 s, and the currents at the outlet increase to 1.5 times the original one. There are CHCs in the output currents of IBDG1 after 0.3 s. Due to the inherent delay of FFT operation, the amplitude of the CHC reaches stability after one cycle, and the stable value is approximately equal to the amplitude of characteristic harmonic signals, as shown in Figure 13. From Figure 12, the distortion rate of CHC is stabilized at 4%. The above simulation results are consistent with the theoretical analysis in Section 3 and can verify the correctness of the CHCs injection system under the fault.

6.3. Verifying the Correctness of IHCDP

6.3.1. Case 1: Asymmetrical Short-Circuit Faults with 0.1 Ω Fault Resistance Occur at f_1

At 0.3 s, set single-phase-to-ground (A–G) faults, two-phase-to-ground (AB–G) faults, and phase-to-phase (A–B) faults with 0.1 Ω fault resistance occur at f_1 , respectively. After detecting faults, IBDG1 and IBDG2 inject CHCs into the distribution network according to the injection strategy. The distortion rates of NSCCHCs on both sides of protected feeder B1B2 after faults are shown in Figure 14.

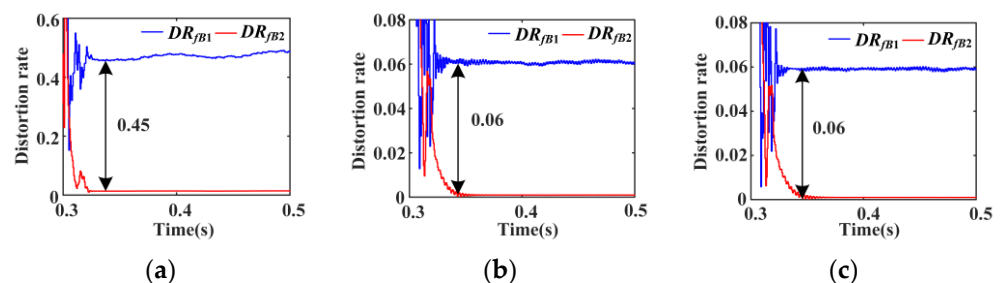


Figure 14. Distortion rate records of asymmetric faults with 0.1 Ω fault resistance. (a) A–G fault, (b) AB–G fault, and (c) A–B fault.

In Figure 14, DR_{fb1} and DR_{fb2} represent the distortion rates of NSCCHCs on the GRID and IBDG sides of protected feeder B1B2, respectively. The action threshold of NSCCHCs differential protection criterion is set to 2%. From Figure 14, when the A–G, AB–G, and

A–B faults occur at f_1 , the distortion rate difference values of NSCCHCs on both sides of feeder B1B2 are about 0.45, 0.06, and 0.06 after one cycle. It can be seen that the IHCDP can sensitively trip under various asymmetric faults, especially under single-phase-to-ground faults.

6.3.2. Case 2: Symmetrical Short-Circuit Faults with 0.1Ω Fault Resistance Occur at f_1

On the basis of Case 1, the fault types at point f_1 are changed to three-phase faults with 0.1Ω fault resistance. Distortion rates of A-phase CHCs on both sides of feeder B1B2 after the fault are shown in Figure 15.

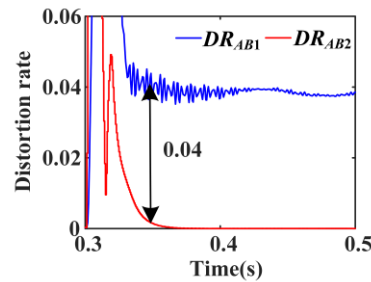


Figure 15. Distortion rates of the A-phase CHCs under the three-phase fault with 0.1Ω .

In Figure 15, DR_{AB1} and DR_{AB2} represent the distortion rates of A-phase CHCs on the GRID and IBDG sides, respectively. The action threshold of the A-phase CHC differential protection criterion is set to 2%. From Figure 15, when a three-phase fault occurs at f_1 , the distortion rate difference value of A-phase CHCs on both sides of feeder B1B2 is about 0.04 after stabilization, which is greater than the action threshold. The above simulation results are consistent with the theoretical analysis in Section 5, and IHCDP can reliably trip under symmetrical short-circuit faults.

6.3.3. Case 3: Asymmetrical Short-Circuit Faults with 20Ω Fault Resistance Occur at f_1

On the basis of Case 1, the fault resistance at point f_1 is changed to 20Ω . Distortion rates of NSCCHCs on both sides of feeder B1B2 after faults are shown in Figure 16.

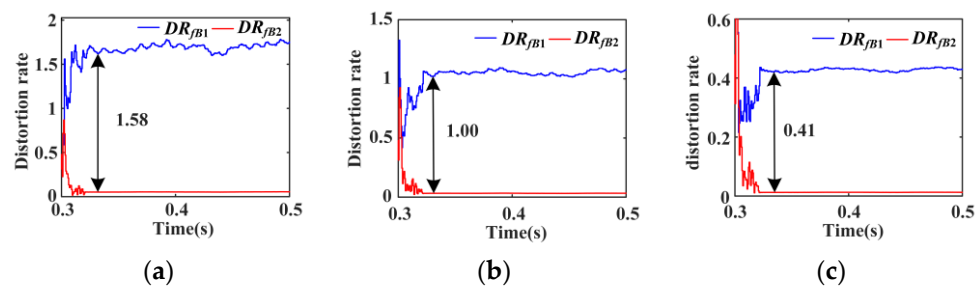


Figure 16. Distortion rate records of asymmetric faults with 20Ω fault resistance. (a) A–G fault, (b) AB–G fault, and (c) A–B fault.

From Figure 16, when the A–G, AB–G, and A–B faults occur at f_1 , the distortion rate difference values of NSCCHCs on both sides of feeder B1B2 are about 1.58, 1.00, and 0.45 after one cycle. The distortion rate difference values under high-resistance asymmetric faults are much larger than the action threshold. Due to the large fault resistance leading to a small NSCFFC, the distortion rate of NSCCHC on the IBDG side is larger. In conclusion, the IHCDP, under various asymmetric faults with high fault resistance, can reliably trip with high sensitivity.

6.3.4. Case 4: Symmetrical Short-Circuit Faults with 20 Ω Fault Resistance Occur at f_1

On the basis of Case 2, the fault resistance at point f_1 is changed to 20 Ω. The distortion rates of A-phase CHCs on both sides of feeder B1B2 after the fault are shown in Figure 17.

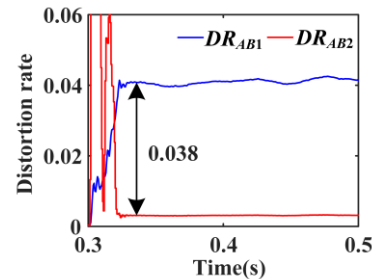


Figure 17. Distortion rates of the A-phase CHCs under the three-phase fault with 20 Ω fault resistance.

From Figure 17, the difference value of the A-phase CHC distortion rates on both sides is about 3.8% after stabilization, slightly lower than 4%. This is due to the large fault resistance at the fault point, which makes most CHCs flow to the fault point f_1 and another small part to the GRID downstream of the fault point. The IHCDP can trip reliably under symmetrical faults with high fault resistance.

Taking feeder B2B3 as the protected section, different types (A–G, AB–G, A–B, and ABC) of faults with different fault resistances (0.1 Ω, 20 Ω, and 50 Ω) are set at point f_2 and the simulation results are shown in Table 2. It can be seen from Table 2 that the proposed protection scheme can sensitively and reliably trip under different fault conditions and has a strong ability to withstand fault resistance.

Table 2. Simulation results of faults with high fault resistance occur at f_2 .

Fault Resistance	Fault Type	Distortion Rate Difference Values	Trip or Not
0.1 Ω	A–G	0.18	Yes
	AB–G	0.06	Yes
	A–B	0.055	Yes
	ABC	0.04	Yes
20 Ω	A–G	0.52	Yes
	AB–G	0.34	Yes
	A–B	0.15	Yes
	ABC	0.035	Yes
50 Ω	A–G	1.14	Yes
	AB–G	0.87	Yes
	A–B	0.33	Yes
	ABC	0.036	Yes

7. Conclusions

Based on the idea of control-protection synergy, this paper investigates the CHC injection protection scheme for the distribution network with IBDGs. The contribution of this paper can be summarized as follows:

- (1) The CHC injection-control strategy of IBDG based on the d-axis and q-axis is proposed. Injection starting criteria are established based on the mutation of phase current and voltage.
- (2) The fault characteristics of CHCs after injection are analyzed. For asymmetrical short-circuit faults, a differential protection criterion based on the distortion rate of NSCCHCs is proposed; for symmetrical short-circuit faults, the proposed differential protection criterion utilizes the distortion rate of A-phase CHCs.

Theoretical analysis and simulation experiments show that the proposed CHC injection system can accurately and reliably operate under normal operation or fault conditions;

the proposed IHCDP can sensitively and reliably trip under symmetrical or asymmetrical faults and has a solid ability to withstand high transition resistance.

Author Contributions: Conceptualization, C.Y. and Z.G.; data curation, C.Y. and Z.L.; formal analysis, C.Y., Z.G. and Z.T.; funding acquisition, Z.G.; methodology, C.Y., Z.G. and Z.L.; project administration, Z.G.; software, C.Y.; validation, C.Y. and Z.G.; visualization, C.Y. and Z.T.; writing original draft, C.Y.; writing review and editing, C.Y., Z.G. and Z.L. All authors have read and agreed to the published version of the manuscript.

Funding: This work was supported in part by the Science and Technology Project of State Grid Corporation of China (52060019001H).

Institutional Review Board Statement: Not applicable.

Informed Consent Statement: Not applicable.

Data Availability Statement: The data presented in this study are available in the article.

Conflicts of Interest: The authors declare no conflict of interest. The funders had no role in the design of the study; in the collection, analyses, or interpretation of data; in the writing of the manuscript or in the decision to publish the results.

References

1. Barani, M.; Aghaei, J.; Akbari, M.A.; Niknam, T.; Farahmand, H.; Korpas, M. Optimal Partitioning of Smart Distribution Systems into Supply-Sufficient Microgrids. *IEEE Trans. Smart Grid* **2019**, *10*, 2523–2533. [\[CrossRef\]](#)
2. Telukunta, V.; Pradhan, J.; Agrawal, A.; Singh, M.; Srivani, S.G. Protection Challenges Under Bulk Penetration of Renewable Energy Resources in Power Systems: A Review. *CSEE J. Power Energy Syst.* **2017**, *3*, 365–379. [\[CrossRef\]](#)
3. Jamali, S.; Borhani-Bahabadi, H. Protection Method for Radial Distribution Systems with DG Using Local Voltage Measurements. *IEEE Trans. Power Del.* **2019**, *34*, 651–660. [\[CrossRef\]](#)
4. Zhang, F.; Mu, L.; Wang, Z.; Zhou, H.; Zhang, X. Optimal Fault Control Strategy of Master-slave Controlled Islanding Microgrid. *Proc. CSEE* **2020**, *40*, 1241–1248.
5. Eskandari, M.; Savkin, A.V. On the Impact of Fault Ride-Through on Transient Stability of Autonomous Microgrids: Nonlinear Analysis and Solution. *IEEE Trans. Smart Grid* **2021**, *12*, 999–1010. [\[CrossRef\]](#)
6. Coffele, F.; Booth, C.; Dysko, A. An Adaptive Overcurrent Protection Scheme for Distribution Networks. *IEEE Trans. Power Del.* **2015**, *30*, 561–568. [\[CrossRef\]](#)
7. Kumar, D.S.; Srinivasan, D.; Reindl, T. A Fast and Scalable Protection Scheme for Distribution Networks with Distributed Generation. *IEEE Trans. Power Del.* **2016**, *31*, 67–75. [\[CrossRef\]](#)
8. Shen, S.; Lin, D.; Wang, H.; Hu, P.; Jiang, K.; Lin, D.; He, B. An Adaptive Protection Scheme for Distribution Systems with DGs Based on Optimized Thevenin Equivalent Parameters Estimation. *IEEE Trans. Power Del.* **2017**, *32*, 411–419. [\[CrossRef\]](#)
9. Darabi, A.; Bagheri, M.; Gharehpetian, G.B. Highly reliable overcurrent protection scheme for highly meshed power systems. *Int. J. Electr. Power Energy Syst.* **2020**, *119*, 105874. [\[CrossRef\]](#)
10. Ma, J.; Liu, J.; Yang, G.; Phadke, A.G. Research on regional centralized protection scheme for distribution network integrated with electric vehicles. *Int. J. Electr. Power Energy Syst.* **2020**, *119*, 105903. [\[CrossRef\]](#)
11. Ghotbi-Maleki, M.; Chabanloo, R.M.; Zeineldin, H.H.; Miangafsheh, S.M.H. Design of Setting Group-Based Overcurrent Protection Scheme for Active Distribution Networks Using MILP. *IEEE Trans. Smart Grid* **2021**, *12*, 1185–1193. [\[CrossRef\]](#)
12. Mirshekali, H.; Dashti, R.; Keshavarz, A.; Torabi, A.J.; Shaker, H.R. A Novel Fault Location Methodology for Smart Distribution Networks. *IEEE Trans. Smart Grid* **2021**, *12*, 1277–1288. [\[CrossRef\]](#)
13. Jamali, S.; Borhani-Bahabadi, H. Non-communication protection method for meshed and radial distribution networks with synchronous-based DG. *Int. J. Electr. Power Energy Syst.* **2017**, *93*, 468–478. [\[CrossRef\]](#)
14. Jia, K.; Bi, T.; Ren, Z.; Thomas, D.W.P.; Sumner, M. High Frequency Impedance Based Fault Location in Distribution System with DGs. *IEEE Trans. Smart Grid* **2018**, *9*, 807–816. [\[CrossRef\]](#)
15. Chen, G.; Liu, Y.; Yang, Q. Impedance Differential Protection for Active Distribution Network. *IEEE Trans. Power Del.* **2020**, *35*, 25–36. [\[CrossRef\]](#)
16. Sharma, N.K.; Samantaray, S.R. PMU Assisted Integrated Impedance Angle-Based Microgrid Protection Scheme. *IEEE Trans. Power Del.* **2020**, *35*, 183–193. [\[CrossRef\]](#)
17. Gao, H.; Li, J.; Xu, B. Principle and Implementation of Current Differential Protection in Distribution Networks with High Penetration of DGs. *IEEE Trans. Power Del.* **2017**, *32*, 565–574. [\[CrossRef\]](#)
18. Zhou, C.; Zou, G.; Du, X.; Zang, L. Adaptive current differential protection for active distribution network considering time synchronization error. *Int. J. Electr. Power Energy Syst.* **2022**, *140*, 108085. [\[CrossRef\]](#)
19. Laaksonen, H.J. Protection Principles for Future Microgrids. *IEEE Trans. Power Electron.* **2010**, *25*, 2910–2918. [\[CrossRef\]](#)

20. Azzouz, M.A.; Hooshyar, A. Dual Current Control of Inverter–Interfaced Renewable Energy Sources for Precise Phase Selection. *IEEE Trans. Smart Grid* **2019**, *10*, 5092–5102. [[CrossRef](#)]
21. Song, G.; Wang, T.; Zhang, B.; Dong, X.; Kang, X. Analysis and Prospect of Detective Fault Identification Technologies Using Power Electronic Device. *Autom. Electr. Power Syst.* **2020**, *44*, 173–188.
22. Soleimanisardoo, A.; Karegar, H.K.; Zeineldin, H.H. Differential Frequency Protection Scheme Based on Off–Nominal Frequency Injections for Inverter–Based Islanded Microgrids. *IEEE Trans. Smart Grid* **2019**, *10*, 2107–2114. [[CrossRef](#)]
23. El–Sayed, W.T.; Azzouz, M.A.; Zeineldin, H.H.; El–Saadany, E.F. A Harmonic Time–Current–Voltage Directional Relay for Optimal Protection Coordination of Inverter–Based Islanded Microgrids. *IEEE Trans. Smart Grid* **2021**, *12*, 1904–1917. [[CrossRef](#)]
24. Guo, W.; Mu, L.; Zhang, X. Fault Models of Inverter–Interfaced Distributed Generators within a Low–Voltage Microgrid. *IEEE Trans. Power Del.* **2017**, *32*, 453–461. [[CrossRef](#)]
25. Blaabjerg, F.; Teodorescu, R.; Liserre, M.; Timbus, A.V. Overview of control and grid synchronization for distributed power generation systems. *IEEE Trans. Power Electron.* **2006**, *53*, 1398–1409. [[CrossRef](#)]
26. Kong, X.; Zhang, Z.; Yin, X.; Wang, F.; He, M. Study on Fault Current Characteristics and Fault Analysis Method of Power Grid with Inverter Interfaced Distributed Generation. *Proc. CSEE* **2013**, *33*, 65–74.
27. Zhang, F.; Mu, L. A Fault Detection Method of Microgrids with Grid–Connected Inverter Interfaced Distributed Generators Based on the PQ Control Strategy. *IEEE Trans. Smart Grid* **2019**, *10*, 4816–4826. [[CrossRef](#)]
28. Bae, Y.; Trung–Kien, V.; Kim, R. –Y. Implemental Control Strategy for Grid Stabilization of Grid–Connected PV System Based on German Grid Code in Symmetrical Low–to–Medium Voltage Network. *IEEE Trans. Energy Convers.* **2013**, *28*, 619–631. [[CrossRef](#)]
29. *China National Standard GB/T 19964–2012*; Technical Requirements for Connecting Photovoltaic Power Station to Power System. Standardization Administration of China: Beijing, China, 2012.
30. Zhao, F.; Meng, Z.; Li, Y.; Liu, C. Pilot Protection Scheme for Active Distribution Network Based on Fault Components. *High Volt. Eng.* **2019**, *45*, 3092–3100.
31. Han, H.; Mu, L.; Zhang, F.; Guo, W. Microgrid Protection Considering Low Voltage Ride-through of IIDG. *Proc. CSEE* **2017**, *37*, 110–119.
32. Han, B.; Li, H.; Wang, G.; Zeng, D.; Liang, Y. A Virtual Multi–Terminal Current Differential Protection Scheme for Distribution Networks with Inverter–Interfaced Distributed Generators. *IEEE Trans. Smart Grid* **2018**, *9*, 5418–5431. [[CrossRef](#)]
33. *China National Standard NB/T 32004–2018*; Technical Specification of PV Grid–Connected Inverter. Standardization Administration of China: Beijing, China, 2018.
34. Svensson, J.; Bongiorno, M.; Sannino, A. Practical implementation of delayed signal cancellation method for phase–sequence separation. *IEEE Trans. Power Del.* **2007**, *22*, 18–26. [[CrossRef](#)]
35. *China National Standard GB/T 156–2017*; Standard Voltages. Standardization Administration of China: Beijing, China, 2017.

Disclaimer/Publisher’s Note: The statements, opinions and data contained in all publications are solely those of the individual author(s) and contributor(s) and not of MDPI and/or the editor(s). MDPI and/or the editor(s) disclaim responsibility for any injury to people or property resulting from any ideas, methods, instructions or products referred to in the content.